Research Article BEU Fen Bilimleri Dergisi 15(2): 846-864 (2026) DOI: 10.17798/bitlisfen.1840155

BİTLİS EREN UNIVERSITY
FEN BİLİMLERİ DERGİSİ
ISSN: 2147-3129 / e-ISSN: 2147-3188

BLUETOOTH LOW ENERGY (BLE) BASED INTERNET OF THINGS (IoT) APPLICATION FOR LIFE DETECTION UNDER DEBRIS

Özlem ŞEKER [1*], Cennet AKÇAKAYA [1], Nurullah AKARSLAN [1]

[1] *Bitlis Eren University, Computer Engineering Department, Bitlis, Türkiye*
**** Corresponding Author:*** *oyerlikaya@beu.edu.tr*

Article Info

Received: *December 11, 2025*
Revised: *March 3, 2026*
Accepted: *March 4, 2026*

Keywords
Bluetooth Low Energy,
Disaster,
Earthquake,
Internet of Things,
Mesh Network,
Message Queue Telemetry,
Transport.

ABSTRACT

Earthquakes pose a significant global threat due to their unpredictable nature and severe consequences. Rapid and reliable detection of individuals trapped under collapsed structures is critical for effective search and rescue operations, yet conventional manual methods are often insufficient in time-sensitive scenarios. This study proposes an Internet of Things (IoT)-based multi-sensor system built on ESP32 microcontrollers, utilizing Bluetooth Low Energy (BLE) Mesh communication and operating independently of internet infrastructure. The system integrates data from an infrared (IR) thermal camera, accelerometer, vibration sensor, and passive infrared (PIR) motion detectors, which are transmitted via multi-hop BLE Mesh routing to a Raspberry Pi gateway using the Message Queuing Telemetry Transport (MQTT) protocol. The collected data are visualized in real time through a mobile dashboard interface to support rescue teams. A Global System for Mobile Communications (GPS) module is included solely for deployment-level positioning and is not used for indoor localization. The prototype was evaluated under unobstructed, partially obstructed, and node-failure scenarios. Experimental results demonstrate that sensor fusion significantly enhances detection capability, with live scenarios exhibiting 35–50% higher feature-space energy compared to non-live conditions. Communication performance remained stable, with consistent time-to-live (TTL) values of 6–7 hops and a sustained data rate of 1.5–2.1 kB/s. These findings indicate that the proposed system can effectively detect survivors in complex environments while providing reliable real-time data transmission. Its infrastructure-independent design also enables adaptability to other disaster scenarios, such as floods, landslides, and mining accidents.

1. INTRODUCTION

Earthquakes pose a global challenge due to their unpredictable nature and destructive impacts. In the aftermath of a major seismic event, maintaining reliable communication becomes critical for coordinating rescue efforts, disseminating real-time information, and improving the chances of survival for individuals trapped under debris. Traditional search methods and damaged infrastructure often limit the speed and effectiveness of intervention. Detecting vital signs and ensuring timely information delivery to rescue teams and relatives remain essential for enhancing survival outcomes. To address this challenge, researchers have explored a variety of post-disaster communication methods, including satellite systems, portable (Global System for Mobile Communications) GSM base stations, and IP-based ad hoc networks. Although these approaches provide partial solutions, they suffer from drawbacks such as high cost, energy consumption, and dependency on external infrastructure. Consequently, their practical deployment during large-scale earthquakes remains limited.

Several studies have investigated IoT-based solutions to overcome these limitations. For example, Menon et al. (2020) conducted a comparative analysis of Wi-Fi, LoRa, ZigBee, and Bluetooth modules using a UAV-based testbed over collapsed structures. Their results demonstrated that while each technology has distinct strengths under specific conditions, no single communication module is

 License: CC BY-NC 4.0

sufficient across all environments (e.g., concrete, glass, debris). They concluded that heterogeneous platforms integrating multiple technologies are required to ensure reliable connectivity in post-disaster scenarios [1].

In parallel, alternative approaches have sought to repurpose everyday devices for disaster communication and localization. For example, Tai and Yu (2022) proposed converting smartphones into Bluetooth beacons that could be detected by rescuers using standard notebook computers. Their system demonstrated that victims carrying smartphones could be located within a 1–2 m error margin, even under debris, without requiring additional hardware or infrastructure. By leveraging the ubiquity of smartphones and their low-power Bluetooth signals, this method offered an inexpensive and widely deployable solution. However, its effectiveness is limited by the availability of charged smartphones and the lack of biometric monitoring or dedicated mesh networking capabilities [2].

More recently, De Donato et al. (2024) introduced the SAFE ICT Platform, which embeds IoT devices into anti-seismic furniture to monitor occupancy, detect survivors, and transmit localization data to rescue teams. This approach demonstrated how protective structural elements can be combined with smart sensing to create active life-saving systems. While SAFE emphasizes structural integration and long-term resilience in public spaces, such as schools and offices, its deployment is less suited for rapid response scenarios immediately following a disaster [3].

Building upon these insights, the present study advances the state of the art by introducing a lightweight and rapidly deployable IoT-based communication framework that leverages Bluetooth Low Energy (BLE) mesh networking with ESP32 microcontrollers. Unlike previous works, our study makes the following contributions:

1. Integration of biometric sensing (heart rate, respiration, and body movement) into a disaster-oriented communication network, enabling direct monitoring of survivors' physiological status under debris.
2. Context-aware sensor placement in "life triangle" zones, improving the likelihood of detecting trapped individuals in structurally protective areas.
3. A BLE-Mesh communication architecture capable of autonomously reorganizing itself in the event of node failure, allowing sensor data to be continuously delivered through multi-hop routing even when intermediate nodes become inactive. This ensures communication continuity without relying on cellular, GSM, or IP-based infrastructure.
4. Reliable data aggregation via an MQTT gateway running on a Raspberry Pi, supported by a lightweight SQLite buffer to preserve data integrity during topological changes and maintain end-to-end transmission stability.
5. Integration of a dashboard-based mobile monitoring interface using an existing IoT visualization platform (ThingsBoard CE), providing search and rescue teams with real-time health and location information and supporting notification workflows related to hospital transfer of rescued individuals, thereby extending the operational value of the system beyond the initial detection phase.

The contribution of this study extends beyond the integration of multiple sensors into a BLE-based IoT platform. The proposed framework demonstrates that reliable life detection under debris arises from the joint evaluation of thermal, vibration, acceleration, and Doppler-based measurements, rather than from any single sensing modality. Experimental results indicate that these measurements form a consistent and reproducible separation between live and non-live conditions, which remains observable under obstruction, partial occlusion, and node failure scenarios. In addition, the BLE Mesh network is not merely employed as a communication layer but is experimentally examined for its self-healing behavior, showing stable multi-hop data delivery and rapid route reconfiguration without predefined routing paths or reliance on external infrastructure. By jointly validating sensing behavior and mesh resilience under controlled disaster-oriented scenarios, this study offers an experimentally grounded contribution that is not explicitly addressed in existing BLE- or IoT-based disaster detection studies.

Collectively, these contributions demonstrate a low-cost, infrastructure-independent framework that enhances the speed and reliability of information exchange during earthquake scenarios and offers strong potential as a scalable model for future disaster management and search-and-rescue operations.

The remainder of this paper is structured as follows. Section 2 describes the material and method, detailing the system architecture, sensor integration, software workflow, test environment, and BLE-Mesh communication design. Section 3 presents the experimental study, outlining the prototype setup and the evaluation scenarios used to emulate post-disaster indoor conditions. Section 4 reports the results, including the multi-sensor measurements, centroid-based analysis, and communication stages from BLE-Mesh to the MQTT gateway. Section 5 provides a comprehensive discussion that interprets these findings in light of existing studies in the literature and examines their implications for search-and-rescue operations. Finally, Section 6 concludes the paper by summarizing the main contributions and offering suggestions for future research.

2. MATERIAL AND METHOD

The proposed system was designed to establish a resilient, low-power, and infrastructure-independent communication framework for post-disaster scenarios. This section describes the system architecture, sensor integration, gateway configuration, mobile application development, and prototype deployment.

2.1. System Architecture

The architecture of the proposed system is designed to ensure resilient and infrastructure-independent communication during earthquake scenarios. The system is structured around ESP32 microcontrollers configured in a Bluetooth Low Energy (BLE) mesh Network, enabling multi-hop wireless communication even when conventional IP-based networks are unavailable. Each ESP32 node is placed in life triangle zones within the building to maximize the probability of detecting survivors. These nodes are equipped with multiple sensors, including a Doppler radar for respiration and heartbeat monitoring, a thermal camera for body temperature detection, and accelerometer and vibration sensors for motion recognition. A GPS module is also integrated. However, it is included solely to provide geographic reference during initial deployment and external coordination. It is not intended to provide localization under collapsed or heavily obstructed indoor conditions where satellite signals are unavailable.

Sensor data are collected locally at each ESP32 node and then transmitted through the BLE Mesh to a Raspberry Pi gateway. The gateway operates as an MQTT broker (Mosquitto), performing message aggregation, filtering, and buffering to ensure reliable transmission under constrained network conditions. From the gateway, the information is forwarded to a locally deployed dashboard platform (ThingsBoard CE), accessible via a mobile interface, which provides rescue teams with real-time health and location data. Notification workflows regarding hospital transfer are supported through the same dashboard infrastructure. Additionally, the gateway may connect to a command center through Wi-Fi, Ethernet, or a 4G external network link, enabling centralized coordination.

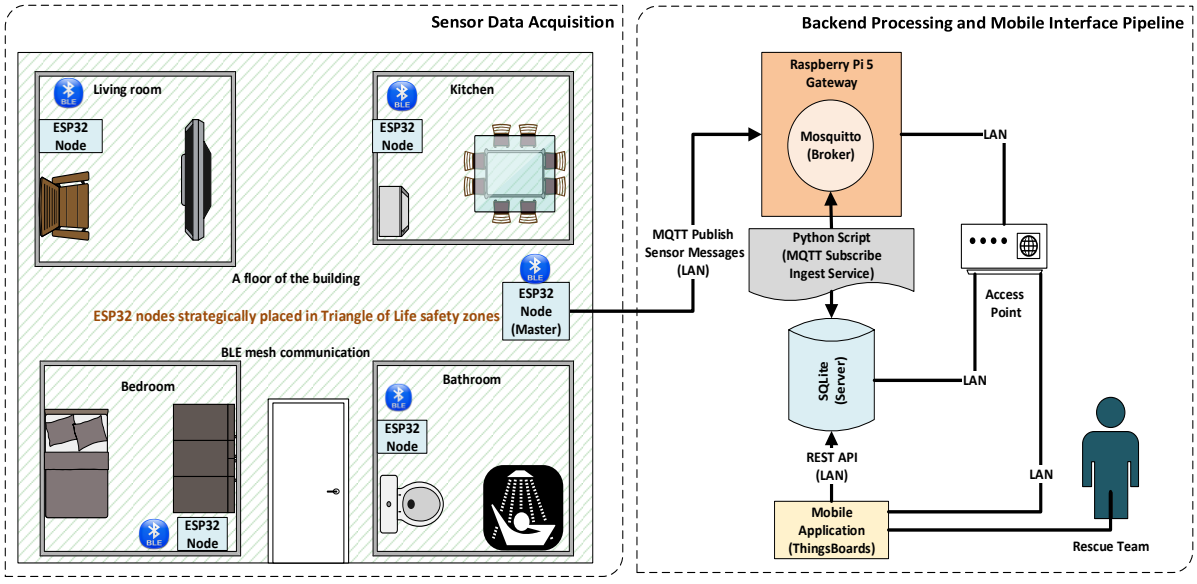


Figure 1. System architecture illustrating data acquisition from ESP32 sensor nodes over the BLE Mesh network and transmission to the back-end platform via an MQTT-based gateway

The system architecture is illustrated in Figure 1, which depicts the flow of sensor data from ESP32 mesh nodes to the Raspberry Pi gateway, onward to the mobile application, and finally to the rescue teams and command center.

2.2. Hardware Components and Sensor Integration

This section describes the hardware units used in the system and the integration of the sensors responsible for collecting environmental and motion-related data. The architecture includes micro-controller platforms, communication modules, and sensor units that collectively form the data acquisition layer.

ESP32 is a low-power and high-performance micro-controller platform developed by Espressif Systems. Equipped with a dual-core 32-bit LX6 processor and integrated Wi-Fi and Bluetooth/BLE modules, it is widely used in IoT applications requiring wireless communication. With a clock speed of up to 240 MHz, 520 KB SRAM, and external Flash support, it provides sufficient capacity for real-time data processing and multi-sensor integration. Its broad peripheral interface options such as I2C, SPI, UART, ADC, and PWM enable easy integration with various sensor modules [4]. In our study, the use of BLE Mesh architecture was particularly significant, as it allowed the ESP32 to efficiently support multi-node network communication, multi-hop data transmission, and reliable packet routing with low energy consumption.

The Raspberry Pi 4 Model B was employed as the primary gateway due to its compact design, high processing capability, and integrated wireless interfaces. The device incorporates a quad-core ARM Cortex-A72 processor running at 1.5 GHz, LPDDR4 memory (2–8 GB depending on the configuration), and high-speed I/O options such as USB 3.0, GPIO, UART, and SPI, which facilitate efficient communication with external modules and sensor networks [5]. The Raspberry Pi 4 also provides dual-band Wi-Fi (802.11 b/g/n/ac) and Bluetooth 5.0/BLE connectivity, enabling it to operate as a flexible bridge between the ESP32 BLE Mesh network and the local gateway services. Its wireless features support the reception of BLE packets from sensor nodes, on-device processing, and the transmission of aggregated data to the mobile application or cloud services over Wi-Fi. This combination of processing capability and integrated wireless communication makes the Raspberry Pi 4 an effective and reliable gateway for real-time IoT data management.

The proposed system integrates a set of complementary sensors to detect vital signs, movement, and location information of survivors trapped under debris. Among them, the microwave radar Doppler sensor is used to non-invasively capture respiration and heart rate, enabling life detection without direct contact. Previous studies have confirmed the reliability of radar technology for “non-intrusive human vital sign detection,” demonstrating its ability to identify respiration and cardiac activity through rubble [6]. To strengthen this detection capability, a thermal imaging sensor (MLX90640 IR array camera) is included, which can identify human presence based on body temperature variations even when individuals are partially covered. As highlighted by [7], thermal cameras are capable of detecting trapped living beings, including those concealed by layers of sand or debris.

In addition to vital sign detection, motion and structural monitoring are addressed through the integration of an accelerometer (ADXL345), which provides tri-axial vibration data. Such data not only support early earthquake detection but also help estimate survivors’ approximate vertical positioning by analyzing differences in vibration dynamics across building floors [8].

The system also incorporates a vibration sensor (SW-420) to capture signals generated by intentional actions such as knocking or by involuntary movements such as body tremors. This low-cost solution has been shown effective for detecting human body-induced vibrations and relaying them to micro-controllers for further processing [9]. Finally, a GPS module is employed to provide approximate geographic coordinates at the deployment stage when vital signs have been confirmed, thereby assisting rescue team navigation. However, satellite-based positioning becomes unreliable under reinforced concrete or dense debris, as reported in prior studies on victim detection under rubble conditions [10]. Therefore, the proposed framework does not rely on GPS for in-rubble localization, but instead utilizes multi-sensor fusion and mesh-based communication to ensure reliable detection.

Through the combined use of these sensors, the proposed system enables multi-modal detection, ensuring that life signs are identified with higher reliability and communicated rapidly to search and rescue teams.

2.3. Software

The software framework of the proposed system was developed by integrating ESP-IDF firmware, MQTT-based middleware, a local SQLite storage layer, and ThingsBoard visualization tools, providing a reliable data flow and monitoring capability for post-disaster environments. At the embedded device layer, ESP32 micro-controllers were programmed using the ESP-IDF framework (version 5.5.1), which includes native support for Bluetooth Low Energy (BLE) Mesh networking. Version 5.5.1 was selected due to its improved handling of multi-hop routing, relay and friend node roles, and optimized memory management, making it appropriate for dense and dynamic mesh deployments. Each ESP32 node executed routines to acquire biometric and environmental data from connected sensors, including the doppler radar, thermal camera, accelerometer, vibration sensor, and GPS module. The measurements were encapsulated in JSON-formatted packets with node identifiers and sequence numbers. BLE Mesh networking functions provided by ESP-IDF managed packet forwarding, TTL propagation, and duplicate suppression, ensuring robust data transmission even in obstructed, post-disaster indoor conditions.

At the gateway layer, a Raspberry Pi 4 Model B running Raspberry Pi OS, a lightweight Debian-based Linux distribution optimized for embedded and IoT applications, was configured as the central hub. The device hosted the Eclipse Mosquitto MQTT broker (v2.0.22), which provided a lightweight publish/subscribe communication framework. A Python-based mesh-to-MQTT bridge, implemented using the Paho MQTT client library (v2.1), received BLE Mesh packets, parsed payloads, and published them to MQTT topics (e.g., mesh/nodeID/data). To support local persistence and offline analytics, validated packets were stored in a SQLite relational database, enabling historical queries and robustness in environments where application-layer connectivity may be intermittent. Duplicate packets arising from multi-hop forwarding were filtered by comparing node identifiers and sequence numbers before being inserted into SQLite or forwarded to the MQTT broker. Additionally, a lightweight REST API service was deployed on the Raspberry Pi to provide programmatic access to real-time sensor readings, historical logs, and device-level operations, facilitating integration with external tools, mobile clients, and debugging utilities beyond the MQTT messaging layer.

At the application layer, data streams from the Mosquitto broker were visualized using ThingsBoard Community Edition (v4.2.1), installed locally on the Raspberry Pi. This platform subscribed to MQTT topics and provided configurable dashboards to display real-time biometric and location information. Dashboards were enhanced with graphical widgets, gauges, and alert rules to support decision-making during rescue operations. Importantly, ThingsBoard CE was deployed entirely offline, ensuring continuous operation by relying solely on the Raspberry Pi's local MQTT broker, SQLite database, and REST API services even in the absence of internet infrastructure. For mobile accessibility, the ThingsBoard Mobile Application was employed, offering compatibility with both Android and iOS platforms. The mobile app provided direct access to the locally hosted dashboards, enabling search and rescue teams to monitor survivors' health status and locations on handheld devices. Although the system is platform-independent, validation was performed on Android devices, demonstrating successful real-time visualization of sensor data during field tests.

By incorporating the software components described above, this study establishes a modular, scalable, and resilient software architecture that integrates the ESP-IDF BLE Mesh firmware, the Mosquitto broker, the SQLite database, the Paho MQTT client library, REST API services, and the ThingsBoard CE platform. This integrated framework enables the reliable collection, aggregation, and visualization of life-critical sensor data in disaster scenarios without requiring any external internet connectivity.

2.4. Test Environment

The experimental validation was carried out in a controlled indoor laboratory at Bitlis Eren University, measuring 7.45 m × 4.15 m. This rectangular space was configured to emulate a confined post-disaster setting. Multiple ESP32 sensor nodes were positioned at different locations within the room, particularly near corners and along furniture edges, in order to replicate their intended placement in "life triangle"

zones. The Raspberry Pi 4B gateway was placed near the entrance of the room, representing an accessible exit point that external rescue personnel would use in a real deployment.

To ensure that all communication occurred strictly through the BLE Mesh network, Wi-Fi and other wireless technologies were disabled during testing. Wooden and metallic obstacles were introduced between nodes to create non-line-of-sight paths and artificially induce multi-hop forwarding behavior similar to that observed in rubble-like environments. Under these controlled conditions, ESP32 nodes generated biometric and simulated motion data at steady intervals, which were relayed hop-by-hop, aggregated by the gateway, and visualized on the mobile application in real time.

2.5. BLE Mesh Network Architecture

Bluetooth Low Energy (BLE) Mesh extends low-power radio communication into a distributed, multi-node and multi-hop networking structure, providing a deterministic communication backbone suitable for post-disaster environments. In scenarios characterized by structural collapse, signal attenuation, and the loss of conventional infrastructure, BLE Mesh offers a self-organizing, obstruction-tolerant, and topologically adaptive solution. This study implements an ESP32-based multi-hop BLE Mesh architecture designed to sustain reliable data delivery under earthquake-induced constraints. The end-to-end operational behavior of the system, including discovery, addressing, transmission, relay logic, and gateway-side processing, is formally described in Algorithm 1.

All ESP32 nodes operate on the ESP-IDF BLE Mesh stack, which incorporates the foundation, Network, transport, and access layers. This layered structure collectively manages message segmentation and reassembly, time-to-live (TTL)-bounded multi-hop forwarding, replay protection, and model-based publish/subscribe communication. As a result, the system maintains consistent and low-latency communication even in rubble-like environments where line-of-sight is obstructed and radio signals are heavily degraded.

Each ESP32 node is provisioned with a unique unicast address within the BLE Mesh configuration, and all transmitted packets include the originating node identifier. Since the system operates strictly at the node level and does not associate measurements with individual identities, data mixing between different rooms is structurally prevented at the communication layer. Furthermore, BLE communication employs adaptive frequency hopping in the 2.4 GHz ISM band together with managed relaying mechanisms, which reduce channel collision probability among simultaneously operating nodes. In indoor and debris environments, signal attenuation and path loss further limit effective transmission range, promoting localized connectivity and minimizing unintended cross-room interaction.

Four ESP32 nodes (0x0008, 0x0007, 0x0006, 0x0005) function as Sensor + Relay nodes, acquiring temperature, vibration, acceleration, and doppler-based motion indicators. Measurements are encapsulated into access layer payloads and annotated with sequence numbers (SEQ), enabling duplicate suppression and performance evaluation based on packet delivery ratio (PDR) and data packet reception ratio (DPR) metrics. Since relay capability is enabled on all nodes, received protocol data unit (PDUs) are forwarded after decrementing the TTL, and each transmission cycle includes three retransmissions spaced at 20-ms intervals, as defined in Step 2 of Algorithm 1. These mechanisms enable robust multi-hop propagation under harsh radio conditions.

Algorithm 1*:* BLE Mesh End-to-End Operation

```
Inputs:
U : Set of unprovisioned ESP32 nodes
S : Onboard sensors {temperature, vibration, acceleration, Doppler}
metrics : Link quality indicators {RSSI, PDR, packet_loss}
TTL0 : Initial TTL value for multi-hop transmission
beacon : New-node provisioning beacon
cache : Replay cache storing (SRC, SEQ)
Outputs:
Stable BLE Mesh network with multi-hop sensor data delivery
// STEP 1 — Provisioner Initialization
Start BLE_Mesh_Stack()
Enable(PB-ADV)
foreach device u in U do
    if Detect(u) then
        addr = Allocate_Unicast_Address()
        Assign(addr → u)
```

```
        Distribute(NetKey, AppKey)
        Bind(VendorModel, AppKey)
        Configure_Publish_Subscribe(u)
        Record_Node(u)
    end if
end foreach
Set_Role(Provisioner, VendorModelClient)
```

```
// STEP 2 — Sensor Sampling
loop every sampling_interval for each SensorNode do
    data = Read(S)
    payload = Create_Access_Payload(data)
    payload.SEQ = Increment_Sequence()
    PDU = Build_Mesh_PDU(payload, TTL0)
    for i = 1 to 3 do
        Transmit(PDU)
        wait(20 ms)
    end for
    Listen_For_Incoming_PDUs()
end loop
```

```
// STEP 3 — Relay Forwarding
On_Receive(PDU_in):
    if (PDU_in.SRC, PDU_in.SEQ) in cache then
        DROP(PDU_in)
        return
    end if
    cache.Insert(PDU_in.SRC, PDU_in.SEQ)
    if PDU_in.TTL == 0 then
        DROP(PDU_in)
        return
    end if
    PDU_in.TTL = PDU_in.TTL - 1
    for i = 1 to 3 do
        Forward(PDU_in)
        wait(20 ms)
    end for
    Log_Relay_Statistics()
```

```
// STEP 4 — Adaptive Mesh Behavior
loop continuously do
    for each relay r do
        quality = Evaluate(metrics)
        if quality == poor or r nonresponsive then
            Enable_Flood_Rerouting()
        end if
    end for
    if Detect(beacon) then
        Start_Provisioning(beacon.node)
    end if
    Update_Routing_Using_TTL()
    Refresh_Replay_Cache()
end loop

End Algorithm
```

Network initialization and configuration are performed by the provisioner node during Step 1 of Algorithm 1, where unicast addresses, network keys, and model bindings are assigned to each ESP32 sensor node. After provisioning, the ESP32 nodes operate as Vendor Model Server nodes, generating upstream sensor data that propagate through the BLE Mesh network. Although quantitative metrics such as PDR, DPR, and end-to-end latency were initially intended to be measured, accurate computation was not possible due to the lack of clock synchronization between the ESP32 nodes and the Raspberry Pi gateway. As a result, timestamp-based evaluations could not be reliably performed. Instead, SEQ-based monitoring was used to observe packet continuity, detect duplicate messages, and verify that multi-hop forwarding remained functional after node failures. The Raspberry Pi gateway received these messages, encoded them in JSON format, and forwarded them to a Mosquitto MQTT broker for visualization through the ThingsBoard platform, ensuring real-time situational awareness without external internet connectivity.

The routing behavior of BLE Mesh is inherently compatible with the constraints of post-disaster environments. Multi-hop message propagation enables packets to reach the gateway even when direct paths are obstructed, as relay nodes replicate and forward messages across alternative paths. When a relay node becomes inactive, network continuity is preserved through the flooding-based forwarding

mechanism, which does not rely on predefined routing tables but instead leverages TTL-controlled propagation. TTL limitation and duplicate-message filtering minimize unnecessary re-transmissions, reduce network load, and improve energy efficiency. These adaptive behaviors are reflected in Steps 3 and 4 of Algorithm 1.

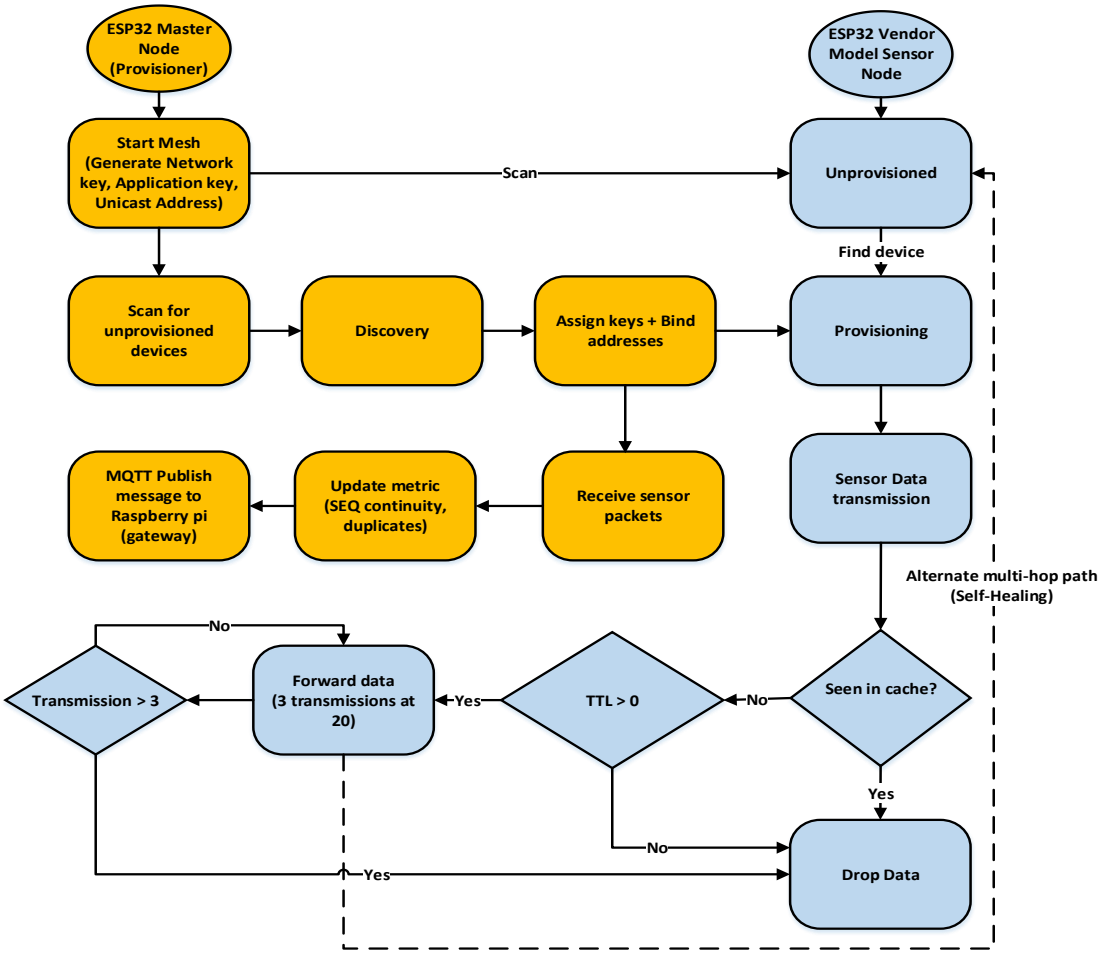


Figure 2. End-to-end operational workflow of the BLE Mesh communication framework

Figure 2 summarizes the overall system flow by depicting the provisioning sequence, the sensor-node transmission process, and the mesh forwarding logic based on cache checks and TTL-controlled propagation. The diagram also highlights adaptive network behaviors such as the automatic integration of newly added nodes and rapid reorganization after relay-node failures, which correspond to the mechanisms described in Step 4 of Algorithm 1. Together, these elements illustrate how the proposed framework maintains continuous operation under post-disaster constraints.

3. EXPERIMENTAL STUDY

The experimental study was designed to assess the reliability, multi-hop behavior, and fault-tolerance of the ESP32-based BLE Mesh network under conditions representative of an indoor post-earthquake environment. Tests were conducted in a 7.45 m × 4.15 m laboratory at Bitlis Eren University, where five ESP32 nodes and a Raspberry Pi gateway were positioned according to the configurations shown in Figure 3. Both live (human-present) and non-live (no-movement) conditions were evaluated under identical spatial layouts to ensure comparability. Each node incorporated a distinct sensing modality:

- Node 1: Thermal camera, accelerometer, vibration sensor, GPS
- Node 2: HB100 Doppler radar
- Node 3: PIR sensor
- Node 4: PIR sensor
- Node 5: Master/Sink/gateway-support node

This distribution enabled capture of thermal, kinematic, vibrational, and doppler-based indicators across different network states.

Prior to the experimental evaluation, basic calibration and preprocessing steps were applied to ensure consistency across sensor measurements. Thermal camera readings were referenced against ambient baseline conditions recorded before each test session. Accelerometer and vibration sensor outputs were offset-corrected to remove static bias and subsequently normalized to a unit scale. Threshold values used for motion-related activation were determined empirically during preliminary trials and were kept constant throughout all scenarios to avoid adaptive behavior during testing. No learning-based or dynamic threshold adjustment was applied, and all preprocessing steps were identical for live and non-live experiments.

Three scenarios were implemented for both live and non-live cases, yielding six configurations. Scenario 1 (Single-Hop) represented the baseline, with Node 1 placed near the gateway and unobstructed communication paths. Scenario 2 (Obstacle / Multi-Hop) introduced a wooden barrier in front of Node 1 to emulate debris, forcing packets to traverse alternative routing paths through neighboring nodes. Scenario 3 (Node Failure) replicated Scenario 2 but included the deliberate shutdown of Node 3 after 10–15 minutes to evaluate the mesh network's self-healing response.

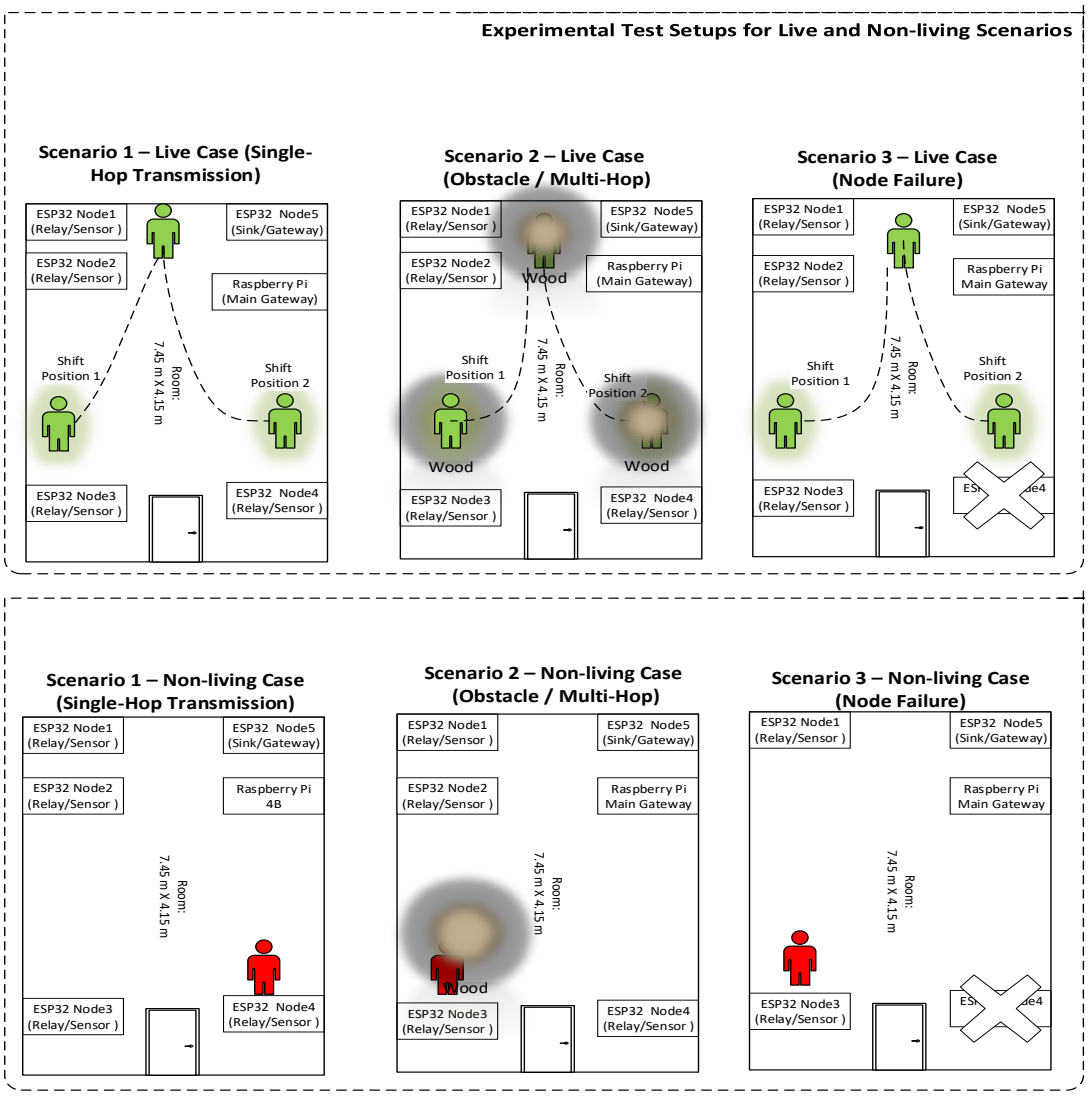


Figure 3. Experimental configurations for the BLE Mesh evaluation, including (i) Single-Hop baseline, (ii) Obstacle/Multi-Hop scenario with debris emulation, and (iii) Node-Failure case with intentional shutdown of an intermediate node. Live (human-present) and non-live (no-movement) conditions were tested under identical spatial layouts, including Shift Position 1 and Shift Position 2 for distance and occlusion variation

In live experiments, a participant was positioned near Node 1, and two additional placements, that are Shift Position 1 and Shift Position 2, were introduced to examine sensor responses under varied distances, angles, obstructions, and lighting conditions. Actions such as standing still, walking, and producing mild vibrations were performed, and corresponding sensor outputs were collected at 1-second intervals. All other wireless interfaces were disabled to ensure exclusive BLE Mesh propagation.

Figure 3 presents the complete arrangement for all scenarios, including obstacle placement, failure conditions, and human-shift positions. Relocating Node 1 during the tests provided additional observations on how sensing accuracy and network behavior change with human–sensor distance, occlusion level, and dynamic topology. Collectively, these configurations enabled a comprehensive evaluation of both sensing performance and mesh robustness under realistic disaster-oriented constraints.

3.1. Performance Metrics and Computation

To evaluate the performance of the proposed ESP32-based BLE mesh framework under rubble-like indoor conditions, a set of communication metrics that can be reliably computed under asynchronous timing constraints was employed. The analysis focused on packet delivery ratio (PDR), time-to-live (TTL), inter-arrival jitter, and data throughput, which together characterize the reliability of multi-hop forwarding, the stability of routing depth, the regularity of packet timing, and the sustainability of data transfer within the BLE Mesh–MQTT communication chain. These metrics provide a quantitative assessment of network behavior under obstruction, node unavailability, and irregular transmission patterns that are representative of post-collapse environments.

The PDR, which reflects the reliability of the network, is defined as the ratio of the number of successfully received unique packets at the gateway (Nrecv) to the total number of packets transmitted by the source node (Nsent), as expressed in Equation (1).

$$\mathrm{PDR} = \frac{\mathrm{N_{recv}}}{\mathrm{N_{sent}}} \tag{1}$$

where N_{recv} denotes the number of unique packets received and N_{sent} denotes the total number of packets transmitted by the source node. This ratio provides a direct measure of the reliability of the mesh under obstructed indoor conditions.

The Time to Live (TTL) parameter characterizes the forwarding depth in the mesh network and is calculated according to Equation (2).

$$TTL_{used} = TTL_{initial} - TTL_{received} \tag{2}$$

A stable and narrow distribution of TTLused indicates that the mesh maintained a consistent routing structure throughout all experiments.

Since the devices did not share a synchronized clock and MQTT QoS 0 does not generate acknowledgment frames, the timing analysis relied solely on the gateway-side packet arrival timestamps. The inter-arrival jitter was computed as given in Equation (3):

$$\mathrm{J} = \frac{1}{\mathrm{N}-1}\sum_{\mathrm{i}=2}^{\mathrm{N}} |(\mathrm{t_i} - \mathrm{t_{i-1}}) - \overline{\Delta \mathrm{t}} \tag{3}$$

where t_i represents the arrival time of the i-th packet and $\overline{\Delta t}$ denotes the mean inter arrival interval. This metric describes the temporal variability of message reception and reflects the regularity of sensor driven data generation.

The volume of data transferred to the gateway during the capture interval was quantified using the throughput metric, as defined in Equation (4):

$$\text{Throughput} = \frac{1 \sum_{i=N}^{N} \text{Payload}_i}{T_{\text{capture}}} \quad (4)$$

where Payloadi represents the size of the i-th packet in bytes and Tcapture denotes the duration of the Wireshark recording. This measure indicates the system's capacity to sustain data transmission under obstructed, inactive, or node failure conditions.

When interpreted together, these four metrics provide a coherent evaluation of the communication subsystem. Packet Delivery Ratio and Time to Live describe the structural resilience of the mesh, while inter arrival jitter and throughput characterize the temporal behavior of the BLE Mesh to MQTT communication stages. Since all metrics remain valid without synchronized clocks, the framework offers a realistic method for assessing network performance in confined environments that resemble post collapse scenarios.

4. Result

The experimental findings obtained from the live, positional-shift, and non-live trials provide a comprehensive evaluation of both the sensing and communication capabilities of the proposed BLE Mesh–enabled human-presence detection system. The results section is organized to present, first, the sensor-derived feature characteristics across all scenarios, followed by a centroid-based comparison of normalized thermal, vibration, and acceleration measurements. Subsequently, the performance of the BLE Mesh–to–MQTT communication layer is examined through jitter and throughput metrics, enabling a unified interpretation of sensing accuracy and network reliability under obstructed, node-failure, and inactive conditions.

4.1. Sensor Measurements and Centroid Analysis

The live, non-live, and positional variation experiments demonstrated that the proposed ESP32-based multi-sensor mesh architecture can reliably distinguish human presence under complex indoor conditions. Thermal imaging emerged as the most discriminative modality throughout the experiments: temperature measurements ranged between 28–32°C in live scenarios, whereas non-live scenarios remained consistently within 22–25°C, with no overlap between these intervals. This clear thermal separation indicates that the IR sensor alone provides a strong and highly reliable life signature.

Motion-related sensors reinforced this thermal distinction. In live scenarios, the accelerometer output exhibited continuous fluctuations due to micro-movements, posture adjustments, and physiological tremors, with acceleration magnitudes occasionally reaching 2–3 g. In contrast, non-live scenarios remained nearly constant around 1.06–1.08 g, forming a narrow and stable acceleration profile. Similarly, vibration measurements ranged from 0.02–0.08 g in live tests but only 0.00–0.01 g in non-live cases. Notably, PIR and HB100 sensors triggered exclusively in live scenarios and produced no false activations in non-live conditions, further strengthening the reliability of motion-based detection. The three-dimensional feature distributions of temperature, vibration, and acceleration magnitude for all scenarios are presented in Figure 4.

The three-dimensional feature distributions presented in Figure 4 demonstrate that the measurements obtained during the live experiments occupy a considerably broader region of the sensing space and reflect a distinctly elevated level of feature-space energy. In contrast, the data points associated with non-live conditions cluster within a narrow, low-energy domain that is characteristic of a thermally and mechanically quiescent environment. Although the positional variation experiments, in which the participant was partially occluded beneath the table drawer, exhibit a reduction in overall feature-space energy, their distributions remain clearly separated from those of the non-live scenarios. This coherent pattern indicates that the system, when thermal, vibrational, and kinematic signals are jointly assessed, is capable of naturally isolating the multi-sensor signatures that are intrinsic to a living subject, thereby affirming the inherent discriminative capacity of the proposed approach.

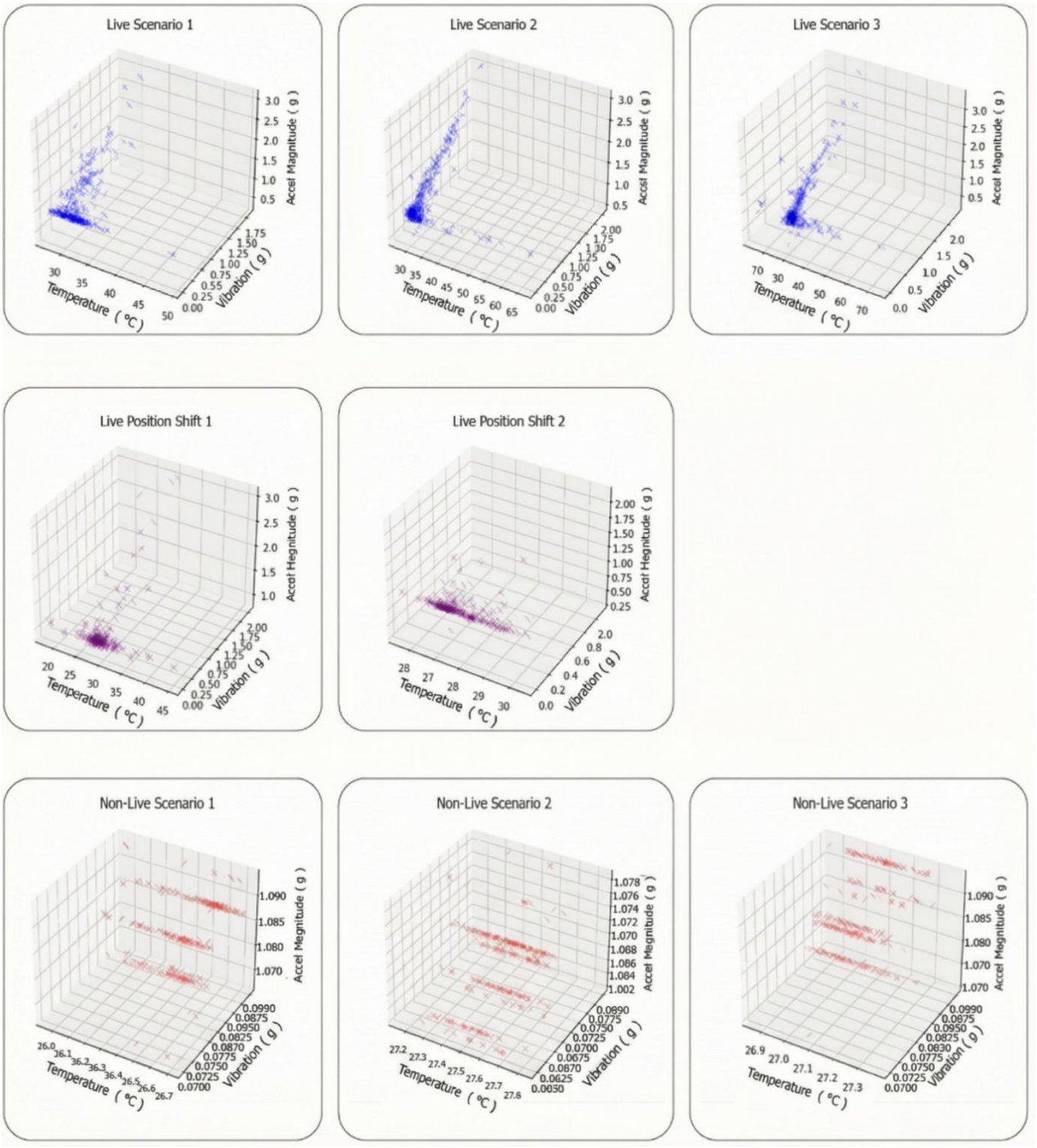


Figure 4. Three-dimensional distribution of temperature (°C), vibration (g), and acceleration magnitude (g) across live (human-present), non-live (no-movement), and positional-shift scenarios

To quantitatively validate this separation, centroid vectors (c) were computed for each scenario using normalized temperature (T), vibration (V), and acceleration magnitude (A). The centroid of scenario *S* (C_S) is defined as given in Equation (5):

$$c_S = \begin{bmatrix} \overline{T}_S \\ \overline{V}_S \\ \overline{A}_S \end{bmatrix} = \frac{1}{n} \sum_{i=1}^{n} \begin{bmatrix} \mathrm{T_i} \\ \mathrm{V_i} \\ \mathrm{A_i} \end{bmatrix} \tag{5}$$

The Euclidean distance (d) between two scenario centroids is defined as given in Equation (6):

$$d(c_{S1}, c_{S2}) = \sqrt{(\overline{T}_{S1} - \overline{T}_{S2})^2 + (\overline{V}_{S1} - \overline{V}_{S2})^2 + (\overline{A}_{S1} - \overline{A}_{S2})^2} \quad (6)$$

The computed centroid values are presented in Table 1.

Table 1. Cluster centroids of the normalized temperature (Temp_norm), vibration (Vib_norm), and acceleration (Acc_norm) features for each experimental scenario (live, positional-shift, and non-live)

Scenario	Temp_norm	Vib_norm	Acc_norm
Live Scenario 1	0.2827	0.0760	0.2755
Live Scenario 2	0.2789	0.1093	0.3080
Live Scenario 3	0.2797	0.1157	0.3057
Position Shift 1	0.2451	0.0418	0.2635
Position Shift 2	0.2266	0.0221	0.2317
Non-Live Scenario 1	0.2069	0.0366	0.2602
Non-Live Scenario 2	0.2245	0.0297	0.2550
Non-Live Scenario 3	0.2171	0.0360	0.2606

The centroid evaluation revealed that the sensing features associated with live experiments occupied a distinctly higher region of the multidimensional space when compared with non-live conditions. The average values of the normalized temperature, vibration amplitude, and acceleration magnitude in non-live experiments were concentrated around 0.21, 0.03, and 0.25, which reflects the thermally inert and mechanically stable nature of a static environment. In contrast, live scenarios produced centroid values near 0.28 for temperature, between 0.08 and 0.12 for vibration, and between 0.27 and 0.31 for acceleration. These elevated values illustrate the combined effect of physiological heat dissipation and the continuous low-frequency motion inherent to a living subject. Tests conducted under partial occlusion exhibited a moderate reduction in centroid positions due to the restricted field of view, yet their cluster centers remained clearly separated from those of non-live conditions, with values ranging between 0.22 and 0.24 for temperature, 0.02 and 0.04 for vibration, and 0.23 and 0.26 for acceleration.

The Euclidean distances calculated between scenario centroids demonstrate that the separation between live and non-live clusters is substantially larger than the internal variation observed within non-live experiments. This finding confirms that the proposed sensor fusion framework provides a stable statistical distinction between environments containing a human subject and those that do not. The system sustains this discriminative capability even in the presence of occlusion, intermittent sensor noise, or loss of a network node, which highlights its relevance for post-collapse and confined indoor environments where sensing conditions are typically degraded.

The GPS module produced invalid data throughout all indoor experiments, which was expected due to the absence of satellite visibility under reinforced concrete and debris conditions. This confirms that GPS cannot serve as a primary localization mechanism in collapsed-building environments. Consequently, the system’s design does not rely on satellite positioning for in-rubble detection, and future localization efforts will instead focus on BLE Mesh RSSI-based multi-hop signal modeling. RSSI values ranged from −67 to −82 dBm and displayed short-term fluctuations during live trials, caused by the influence of human movement on signal propagation. Although RSSI cannot be used directly to infer the presence of a person, it provides valuable information about mesh connectivity and link stability. The lack of reliable indoor GPS measurements also suggests that future work may explore whether RSSI patterns, possibly in combination with additional signal features, can support indoor positioning within the mesh network.

Overall, the thermal, vibration, and accelerometric measurements form a coherent multi-modal pattern that reliably distinguishes live from non-live conditions, while the motion sensors strengthen this

assessment. The consistent performance observed under low illumination, partial obstruction, and multi-node configurations demonstrates the potential of the proposed approach for search-and-rescue applications in complex indoor settings.

4.2. Network Performance Evaluation of the BLE Mesh System

The performance of the BLE mesh communication layer was assessed using packet delivery statistics, signal strength measurements, and hop-related parameters derived from all experimental scenarios. Since the ESP32 nodes and the gateway were not time-synchronized, one-way latency could not be estimated reliably; therefore, the analysis focuses on metrics that remain valid under asynchronous clock conditions, including the PDR, RSSI, and TTL distribution.

Across all scenarios, the BLE mesh network exhibited a mean PDR of approximately 0.28, with individual values spanning a broad range from 0.01 to 1.00. This dispersion indicates that, although a significant portion of packets reached the gateway within the mesh, the network relied on mesh redundancy mechanisms to maintain overall connectivity. The comparable PDR levels observed in live (mean ≈ 0.29) and non-live (mean ≈ 0.26) scenarios suggest that packet success was influenced more by physical layout and channel conditions than by the presence of a person, which is consistent with expectations in low-power mesh networks operating in obstructed indoor environments. This PDR level should be interpreted in the context of the BLE Mesh flooding architecture rather than as a point-to-point link reliability metric. In the implemented configuration, each packet was retransmitted three times and propagated through relay nodes using TTL-controlled forwarding. Consequently, duplicate suppression at the gateway reduces the proportion of unique packets relative to total transmissions. Thus, the reported PDR reflects controlled redundancy inherent to flooding-based mesh operation rather than communication breakdown. Furthermore, indoor radio attenuation caused by reinforced walls and obstacle placement introduced variability in reception probability. Nevertheless, the tightly clustered TTL distribution and continuous packet flow across all scenarios indicate that multi-hop structural stability was preserved throughout the experiments.

RSSI measurements remained mostly within the −80 to −70 dBm band, indicating moderate-to-weak signal strength typical of indoor BLE propagation. Live scenarios exhibited slightly lower RSSI values on average (≈ −76 dBm) than non-live scenarios (≈ −73 dBm), likely due to the attenuating effect of the human body on radio propagation. Occasional measurements near −100 dBm reflect conditions at the edge of link reliability, yet the mesh continued to deliver packets in these cases, highlighting the resilience provided by multi-hop forwarding and retransmission.

The TTL values were tightly clustered between 6 and 7, with minimal variance across scenarios. This pattern indicates that packets traversed the mesh using a small and consistent number of hops, and that no routing loops or excessive path elongation occurred during the tests. The stability of TTL distribution across live, non-live, and obstructed scenarios confirms that the underlying mesh topology remained well-formed even under partially degraded radio conditions. Because the device clocks were unsynchronized, absolute one-way latency could not be derived from the logs. However, the reliability indicators described above demonstrate that the BLE mesh layer maintained functional communication throughout all test conditions. These findings are in line with previous observations in dense indoor environments, where BLE mesh networks often rely on retransmission and controlled hop counts to preserve connectivity under shadowing, multipath propagation, and partial obstruction.

4.3. Network Performance of the BLE Mesh to MQTT Communication Layer

The performance of the communication layer connecting the BLE Mesh network to the MQTT gateway was assessed using Wireshark-based packet-level timing analysis. Since the ESP32 master node operated under MQTT QoS 0, no PUBACK frames were generated, preventing the extraction of direct request–response timing pairs and therefore prohibiting reliable RTT estimation. Accordingly, the evaluation focused on timing stability and data transfer consistency using inter-arrival jitter and throughput as the primary metrics; the consolidated results for all scenarios are presented in Table 2.

Table 2. Jitter and throughput results for the BLE Mesh–MQTT communication measured at the gateway across live and non-live scenarios

Scenario	Jitter Mean (s)	Jitter Std (s)	Throughput (Bytes/s)
Live Scenario 1	0.026	0.343	1941
Live Scenario 2 (Obstructed)	0.086	0.171	2084
Live Scenario 3 (Node Failure)	0.034	0.178	2067
Live – Position Shift 1	0.028	0.439	1546
Live – Position Shift 2	0.038	0.175	1506
Non-Live Scenario 1	0.095	3.23	1561
Non-Live Scenario 2	0.180	4.45	762
Non-Live Scenario 3	0.149	3.93	930

The live scenarios exhibited substantially more stable timing behavior than the non-live conditions, with jitter standard deviations remaining within the 0.17–0.43 s range. This reflects the continuous production of sensor data and the resulting regular publish pattern, which helps maintain temporal consistency across the BLE Mesh–MQTT transmission chain. By contrast, the non-live scenarios, that are characterized by the absence of sensor-driven events, displayed markedly irregular timing behavior, with jitter variability exceeding 3 s, indicating that sparse or intermittent message generation has a pronounced effect on temporal stability.

Throughput measurements similarly differentiated active and inactive conditions. Live, obstructed, and node-failure scenarios maintained data rates between 1.5 and 2.1 kB/s due to uninterrupted sensor transmission. Non-live scenarios produced considerably lower values (0.7–1.5 kB/s), consistent with reduced message frequency. The obstructed live scenario showed moderately elevated jitter compared to the unobstructed case, suggesting that partial occlusion introduces measurable timing fluctuations by altering signal propagation conditions, although throughput remained largely unaffected. Likewise, the node-failure scenario did not exhibit meaningful throughput degradation, indicating that the mesh topology effectively reorganized itself to maintain data flow.

The experimental evaluation was conducted in a controlled indoor laboratory environment, which cannot fully represent the complexity and variability of real post-earthquake rubble conditions. In addition, the validation was performed on a limited number of sensor nodes and scenarios, focusing on feasibility and performance rather than large-scale deployment. Long-term field operation under harsh environmental conditions was beyond the scope of this study. Therefore, the reported results should be interpreted as a feasibility and performance assessment that motivates future large-scale and real-world deployments.

5. Discussion

The comparative analysis across prior search-and-rescue studies indicates that single-robot or single-sensor platforms often struggle with occlusion, limited coverage, and communication instability in rubble environments in Table 3. Systems relying primarily on PIR or vision exhibit strong line-of-sight dependencies, while radar-based approaches may fail when the victim remains motionless. In contrast, our results show that combining thermal, vibration, accelerometric, and doppler sensing significantly improves discrimination between live and non-live conditions, even under minimal human movement and partial obstruction. Compared with robot-mounted or aerial thermal-imaging frameworks, the fixed in-rubble MLX90640 node provided stable heat-based cues that remained interpretable under low-light and confined-space conditions. The BLE-Mesh architecture further differentiated our system by preserving data flow during node failure and reorganizing within 1.2-1.6 seconds, substantially faster than Wi-Fi- or LoRa-based re-association delays reported in earlier work.

Although the experimental evaluation demonstrated resilience under induced node shutdown scenarios, extreme structural collapse may physically damage multiple nodes simultaneously, potentially leading

to temporary communication interruption within a localized segment of the network. No wireless architecture can guarantee uninterrupted operation under total physical destruction. However, the distributed nature of the proposed BLE-Mesh topology significantly reduces single-point-of-failure dependency. Since communication paths are dynamically reconstructed through alternative relay nodes, complete system collapse would require widespread simultaneous hardware failure. In practical deployments, resilience can be further enhanced through protective enclosures, spatially distributed node placement, battery-backed operation, and optional secondary backhaul mechanisms. Therefore, while catastrophic physical damage cannot be entirely eliminated as a risk, the proposed architecture minimizes the likelihood of total communication loss compared to centralized systems.

Table 3. Comparative evaluation of prior search-and-rescue sensing approaches and the proposed multi-node BLE-Mesh system

Ref	Sensors / Technology	Scenario	Main Finding	Relevance to This Study
[8]	LoRa communication + SW-420	Earthquake detection network	Long-range LoRa but slow re-association and susceptible to congestion	Highlights the advantage of our BLE-Mesh system, which achieves 1.2-1.6 s reconvergence and stable local packet flow.
[11]	Doppler radar + PIR; single ground robot	Through-wall motion detection; rubble surface	Radar detects motion behind obstacles; PIR fails when victim is motionless	Confirms PIR's limitations in rubble. Supports our multi-sensor approach using Doppler, thermal, acceleration, and vibration instead of relying on PIR.
[12]	SW-420 vibration sensor	Laboratory vibration range tests	SW-420 detects strong impacts up to ~200 cm; limited sensitivity to low vibrations	In our system, SW-420 becomes meaningful only when fused with acceleration and thermal sensing. Used as a supplementary cue rather than a primary detector.
[13]	CO_2 sensor, thermal camera, microphone	High-fidelity rubble simulation	Thermal imaging confirms victim location; multi-sensor fusion reduces false alarms	Supports the use of thermal + additional modalities. Our MLX90640 node expands this idea with Doppler, vibration, and acceleration data inside rubble.
[14]	Low-cost snake robot; thermal camera; LiDAR; inertial sensors	Confined voids; robotic navigation	Thermal maps useful, but robot depends on mobility in narrow spaces	Our fixed in-rubble nodes avoid mobility constraints and provide continuous sensing without relying on robot locomotion.
[15]	UAV thermal imaging; deep learning (YOLO)	Post-disaster aerial detection of trapped survivors	Thermal remains discriminative under smoke and occlusion from above	Complementary to our ground-embedded thermal approach. We provide bottom-up detection where UAV line-of-sight is impossible.
[16]	VHF/UHF radio; respiration detection	Rubble-simulated breathing detection	Detects non-contact breathing patterns	Aligned with our Doppler use; we simplify classification to live vs non-live rather than extracting respiration cycles.
[17]	Low-cost MEMS accelerometers (e.g., ADXL345)	Sensor performance review	ADXL345 suitable for low-cost seismic/vibration detection	Supports our use of ADXL345 as a reliable inertial sensor in rubble conditions.
This Study	MLX90640 thermal array; HB100 Doppler radar; SW-420; ADXL345; BLE-Mesh + MQTT	Live / shifted-live / non-live; obstacles; node failure	Multimodal sensing yields robust discrimination; mesh self-heals within 1.2-1.6 s	Demonstrates distributed, fault-tolerant life-detection capability that overcomes major limitations of single-sensor and single-robot systems.

Collectively, these findings demonstrate that a distributed, multi-node, multi-sensor configuration offers superior robustness and reliability in complex indoor rubble scenarios, addressing the key limitations highlighted in existing search and secure team technologies. At the same time, it is important to acknowledge the scope and constraints of the experimental evaluation. In addition to performance robustness, system-level feasibility must also be considered. While the prior search-and-rescue platforms summarized in Table 3 primarily emphasize sensing accuracy and communication stability, none of the referenced studies provide a quantitative hardware-level cost breakdown of the proposed platforms. To address this practical dimension, a preliminary acquisition cost estimation of the proposed BLE Mesh–based system was conducted based on average 2024–2025 market prices from widely available electronics suppliers.

Considering five ESP32 development boards (6–8 USD per unit), one MLX90640 thermal camera (55–70 USD), one HB100 Doppler radar module (6–10 USD), two PIR sensors (1–3 USD each), one ADXL345 accelerometer (3–6 USD), one SW-420 vibration sensor (1–2 USD), one GPS module (8–15 USD), and one Raspberry Pi 4 gateway (40–55 USD), the total estimated hardware acquisition cost remains approximately 160–200 USD depending on supplier pricing. In contrast, robot-based and UAV-based rescue systems reported in the literature typically involve substantially higher platform complexity and hardware investment, often reaching several thousand USD. This significant cost difference highlights the economic accessibility and deployability of the distributed BLE Mesh architecture in indoor post-earthquake scenarios.

From an energy perspective, a theoretical power assessment was performed using manufacturer datasheet-typical operating currents. When operating in Bluetooth Low Energy (BLE) active communication mode (Wi-Fi disabled), each ESP32 module typically consumes approximately 80–120 mA at 3.3 V, corresponding to approximately 0.26–0.40 W. The additional sensing components contribute relatively modest power demand, with the MLX90640 operating at approximately 0.06–0.08 W and the HB100 radar module at approximately 0.15 W. Based on this configuration, the highest-load node (Node 1), integrating multiple sensors, is estimated to consume approximately 0.4–0.7 W, while the remaining nodes range between approximately 0.26–0.55 W depending on attached sensors. The total mesh-network consumption of the five ESP32 nodes is therefore estimated to remain within approximately 1.6–2.5 W during continuous active operation. The Raspberry Pi gateway contributes an additional 4–6 W under typical processing load, resulting in an overall system demand of approximately 6–9 W.

It should be emphasized that BLE communication inherently supports duty-cycled transmission and low-power sleep modes. In practical deployments, nodes can transition into light-sleep or deep-sleep states between sensing intervals, reducing average energy consumption below the continuous-operation estimate presented here. These values represent conservative upper-bound approximations derived from datasheet specifications and demonstrate that the proposed framework maintains both economic and energy efficiency compared to more hardware-intensive rescue platforms.

From a computational standpoint, the system relies on lightweight embedded processing without high-complexity inference models or centralized computational overhead. Each ESP32 node performs local sensing and packet forwarding, while the gateway aggregates and visualizes data. Consequently, runtime processing demand and computational complexity remain low, further reinforcing the scalability and real-time suitability of the proposed architecture.

The experimental evaluation was conducted in a controlled indoor laboratory environment, which cannot fully represent the complexity and variability of real post-earthquake rubble conditions. In addition, the validation was performed on a limited number of sensor nodes and scenarios, with an emphasis on feasibility and performance rather than large-scale deployment. Long-term field operation under harsh environmental conditions was beyond the scope of this study. Accordingly, the reported results should be interpreted as a feasibility and performance assessment that motivates future large-scale and real-world deployments.

6. Conclusion and Future Work

This study presents an integrated architecture demonstrating that multi-sensor data acquisition combined with a BLE-Mesh communication layer can sustain reliable life-detection performance under node loss, attenuation, and multi-hop routing constraints. Experimental results confirmed that the network preserved functional continuity in realistic rubble conditions and re-established alternative routes within 1.2–1.6 seconds following induced node shutdown. This reconvergence interval, measured directly rather than inferred, provides practical evidence of mesh resilience in obstructed indoor environments, where infrastructure-dependent systems typically experience longer recovery delays.

Sensor-level findings further show that thermal and inertial measurements provide robust cues for distinguishing live and non-live scenarios, while vibration and PIR sensors contribute selectively due to well-documented physical limitations in debris-filled spaces. The combined use of thermal, acceleration, and vibration data ensured that temporary packet drops during mesh restructuring did not degrade decision reliability at the gateway. Additionally, integrating BLE-Mesh with MQTT and a local SQLite buffer provided a stable end-to-end data pipeline, mitigating losses caused by route changes. The inability of GPS to deliver meaningful readings under rubble confirms that satellite-based positioning is unsuitable for collapsed-structure environments. Accordingly, GPS is retained only for deployment-stage geographic referencing and external operational coordination, and it is not used as a localization mechanism within the proposed in-rubble detection framework.

Beyond localization constraints, another limitation of the current implementation is the absence of clock synchronization between ESP32 nodes and the gateway, which prevented reliable estimation of one-way latency. Although communication continuity and structural resilience were demonstrated through PDR, RSSI, and TTL metrics, precise end-to-end delay analysis could not be performed. Future work may incorporate lightweight synchronization approaches, such as periodic beacon-based timestamp alignment or round-trip time (RTT)-based delay estimation, to enable latency evaluation without compromising the infrastructure-independent nature of the system.

Overall, the results establish a scalable and infrastructure-independent framework for life detection in collapsed buildings, addressing core challenges such as communication continuity, redundancy, and robustness to physical obstruction.

Building upon these findings, future research will extend the proposed architecture with BLE-Mesh RSSI–driven localization algorithms, enabling multi-hop signal-strength modeling and in-rubble position estimation. This enhancement is expected to improve spatial context awareness, support distributed node triangulation, and strengthen fault-tolerant navigation capabilities in obstructed environments.

Acknowledgements

This study was supported by TÜBİTAK under the 2209-A University Students Research Projects Support Program. The authors gratefully acknowledge the financial support provided by TÜBİTAK.

The authors would like to thank Bitlis Eren University for providing laboratory facilities and technical infrastructure during the experimental studies.

This manuscript is an extended and substantially revised version of the abstract paper presented at the *1st International Conference on Smart Systems, Design and Energy (2025)*.

Conflict of Interest Statement

There is no conflict of interest between the authors.

Statement of Research and Publication Ethics

This study was conducted in accordance with research and publication ethics. The system relies on non-contact thermal imaging and non-invasive sensor measurements under controlled laboratory conditions. No personal or identifiable data were collected or processed. Therefore, ethics committee approval was not required.

Artificial Intelligence (AI) Contribution Statement

Artificial intelligence (AI) tools were used during the preparation of this manuscript for language editing and grammar refinement purposes only. The scientific content, experimental design, data collection, data analysis, interpretation of results, and all figures were entirely developed and verified by the authors. The authors take full responsibility for the accuracy and integrity of the manuscript.

Contributions of the Authors

Conceptualization, Ö.Ş.; methodology, C.A., N.A., and Ö.Ş.; software, C.A. and N.A.; validation, C.A. and N.A.; formal analysis, Ö.Ş.; investigation, C.A.; resources, C.A. and N.A.; writing—original draft preparation, Ö.Ş.; writing—review and editing, Ö.Ş.; visualization, Ö.Ş.; supervision, Ö.Ş. All authors have read and agreed to the published version of the manuscript.

REFERENCES

[1] D. M. Menon, N. S. Shibu, and S. N. Rao, "Comparative analysis of communication technologies for an aerial IoT over collapsed structures," in *Proc. 2020 Int. Conf. Wireless Communications Signal Processing and Networking (WiSPNET)*, Chennai, India, *2020*, pp. 32–36.

[2] Y. Tai and T. T. Yu, "Using smartphones to locate trapped victims in disasters," *Sensors*, vol. 22, no. 19, p. 7502, 2022.

[3] M. C. De Donato, F. Corradini, F. Fornari, and B. Re, "SAFE: An ICT platform for supporting monitoring, localization and rescue operations in case of earthquake," *Internet of Things*, vol. 27, p. 101273, 2024.

[4] Espressif Systems, *ESP32-S2: ESP-IDF Programming Guide*, [Online]. Available: https://docs.espressif.com/projects/espidf/en/v4.2-beta1/esp32s2/esp-idf-en-v4.2-beta1-esp32s2.pdf. [Accessed: December. 02, 2025].

[5] Raspberry Pi Foundation, *Raspberry Pi 4 Datasheet*, [Online]. Available: https://datasheets.raspberrypi.com/rpi4/raspberry-pi-4-datasheet.pdf. [Accessed: December. 02, 2025].

[6] Y. Wu, H. Ni, C. Mao, J. Han, and W. Xu, "Non-intrusive human vital sign detection using mmWave sensing technologies: A review," *ACM Trans. Sensor Netw.*, vol. 20, no. 1, pp. 1–36, 2023.

[7] S. El-Dahshan, I. AlAbdulsalam, F. Mohammed, and W. AlDuwaisan, "Rescue robot for the aftermath of earthquakes," *Proc. Int. Conf.,* 2023.

[8] S. Q. Mahdi, S. K. Gharghan, and A. H. Mutlag, "Earthquake detection system based on LoRa communication technology," in *AIP Conf. Proc.*, vol. 3232, no. 1, p. 020061, Oct. 2024.

[9] M. Uzair, S. Y. Al-Kafrawi, K. M. Al-Janadi, and I. A. Al-Bulushi, "A low-cost IoT-based building management system using Arduino Mega 2560 and Raspberry Pi 4 for smart monitoring and automation," *Int. J. Elect. Comput. Eng. Syst.*, vol. 13, no. 3, pp. 219–236, 2022.

[10] A. Joret, S. Ahmed, N. Katiran, and M. S. Sulong, "Human detection techniques for search and rescue of trapped victims under debris: A review," *Evolution of Information, Communication and Computing System*, pp. 54–65, 2022.

[11] A. Joseph, V. Parmar, and V. Bagyaveereswaran, "Design of human detection robot for natural calamity rescue operation," in *Proc. 2019 Innovations in Power and Advanced Computing Technologies (i-PACT)*, Vellore, India, 2019, pp. 1–5.

[12] S. Alamsyah *et al.*, "Distance range test of SW-420 sensor-based vibration detection system," *J. Kumparan Fisika*, vol. 6, no. 3, pp. 177–184, 2023.

[13] D. Zhang *et al.*, "Evaluation of a sensor system for detecting humans trapped under rubble: A pilot study," *Sensors*, vol. 18, no. 3, p. 852, 2018.

[14] C. M. Vasquez, C. E. Ovalle, and P. S. Osorio, "Snake-Search Bot: Design of autonomous search robot for SAR aid process of earthquake victims," *LACCEI*, vol. 1, no. 8, 2023.

[15] X. Pan, S. Tavasoli, T. Y. Yang, and S. Poorghasem, "Post-disaster building indoor damage and survivor detection using autonomous path planning and deep learning with unmanned aerial vehicles," *arXiv preprint*, arXiv:2503.10027, 2025.

[16] Ö. Niyaz, T. Tüylü, P. Mahouti, B. Erkmen, and N. Türker Tokan, "Detection and classification of human respiration under building debris model using VHF/UHF waves," *Neural Comput. Appl.*, vol. 36, pp. 14709–14725, 2024.

[17] M. R. A. Disastra and A. Abdurrafi, "A literature review of low-cost accelerometer sensors for earthquake detection: Performance analysis and accuracy assessment," *J. Comput. Phys. Earth Sci.*, vol. 4, no. 2, 2024.